Thermal Reflow Effect in Multi-Mode Waveguide of S-Bend Resonator With Mode Discrimination

Yong-Jin Kim, Seok-Ho Hong, Jae-Sang Lee, Su-Jin Jeon, Woo June Choi, and Young-Wan Choi

***Abstract*—Polymer-based S-bend optical resonator consisting of multi-mode waveguide has been used as refractive index sensing devices due to their cost-effectiveness and ease of fabrication. However, during fabrication, the thermal reflow that occurs during the baking process and overdevelopment induces an inclination in the sidewalls of the waveguide. The construction of the angled sidewalls can influence the propagation mode properties of the waveguide, such as the evanescent field and loss. Hence, in this study, we designed and analyzed S-bend resonators to investigate the influence of the sidewall slope on the optical modes of the waveguide and the sensing performance of the resonator with respect to the variation of slope angles. The simulation results revealed that, as the sidewall slope deviated from the right angle (90°–65°), the sensitivity of the device increased by a factor of 1.8 due to the field leakage, whereas, the extinction ratio and Q-factor decreased by 54% and 37%, respectively. The results indicated that the sidewall slope induces a trade-off between the resolution and the sensitivity of the S-bend resonator. The findings of this study can be used as a reference for further research on MMW-based optical sensors using polymer materials.**

***Index Terms*—Multi-mode waveguide, optical refractive index sensor, sidewall slope, S-bend resonator, thermal reflow.**

I. Introduction

OPTICAL sensors that measure changes in the refractive index have attracted considerable interest, as they can rapidly and effectively detect gases or biomaterials. In addition, there has been an increase in the need for efficient material detection through the mass production of optical sensors. Integrated label-free optical sensors have been extensively studied with respect to medical, environmental monitoring, and biochemical analysis applications that require sensitive and rapid analysis tools [1]. Accordingly, optical sensor devices with various structures have been proposed, such as the ring resonator [2], [3], micro-disk resonator [4], Mach–Zehnder interferometer [5], [6], Fabry–Perot interferometer [7], optical coupler [8], and surface plasmon resonance sensor [9]. Among them, optical resonator sensors detect changes in the external effective refractive index by measuring the shift in resonant wavelength peaks due to changes such as antigen–antibody reactions, temperature changes, and protein binding in the sensing region [10].

Optical ring resonators have been developed based on single-mode waveguides (SMWs) with low modal dispersion characteristics, low propagation losses, and small sizes, to improve sensitivity [11], [12]. To realize a low fabricating cost and mass production, a multi-mode waveguide (MMW)-based resonator with a line width of several micrometers should be designed [13]. However, it is difficult to use this resonator as a sensor, given that the modal dispersion causes multiple peaks in the output transmission spectrum. An S-bend resonator can be used to solve this problem by removing multiple peaks through the mode discrimination technique, which was presented in a previous study [14].

Mode discrimination is a phenomenon in which the multiple peaks of the transmission spectrum are removed by eliminating the higher-order mode using the difference in the effective refractive index between the fundamental mode and higher-order modes in a specific waveguide structure with propagation loss. The transmission spectrum of the S-bend resonator with mode discrimination has characteristics similar to those of the SMW-based ring resonator. The S-bend resonator is designed based on a MMW with a line width of several micrometers to enable contact lithography. The fabrication process of silicon photonic sensors is basically composed of deposition, photoresist spin coating, E-beam lithography, development, dry etching, and photoresist removal [3]. However, the S-bend resonator that can be fabricated with a polymer uses photolithography instead of E-beam lithography, and deposition, dry etching, and photoresist removal are excluded. Accordingly, it is possible to fabricate at a low cost and also to reduce the fabricating time, thereby enabling mass production. Furthermore, it consists of MMWs that have larger areas of contact with the external environment than those consisting of SMWs. Therefore, it might be effective in terms of measurability and ease of measurement of the substances.

The waveguide constituting the S-bend resonator is designed in a ridge structure using SU-8 polymer (negative photoresist), which is capable of contact lithography and exhibits high optical transparency [15], [16]. However, SU-8 is an amorphous polymer with glass transition characteristics; therefore, it transitions from a glassy state to a rubbery state by heat treatment during the post-exposure bake process for cross-linking after ultraviolet (UV) light exposure in the fabricating process. Under this condition, thermal reflow may occur; this reflow gradually

Manuscript received October 26, 2021; revised December 24, 2021; accepted January 7, 2022. Date of publication January 13, 2022; date of current version January 27, 2022. This work was supported in part by the Basic Science Research Program through the National Research Foundation of Korea funded by the Ministry of Education under Grant NRF-2018R1D1A1B07048145, and in part by the Korea Institute for Advancement of Technology Grant funded by the Korea Government under Grant P0017011, HRD Program for Industrial Innovation. *(Corresponding author: Young-Wan Choi.)*

The authors are with the Department of Electrical and Electronics Engineering, Chung-Ang University, Dongjak-gu, Seoul 06974, Republic of Korea (e-mail: rladydwla321@cau.ac.kr; hoonjis27@cau.ac.kr; lwotkd@cau.ac.kr; jsj0601@cau.ac.kr; cecc78@cau.ac.kr; ychoi@cau.ac.kr).

Digital Object Identifier 10.1109/JPHOT.2022.3142391

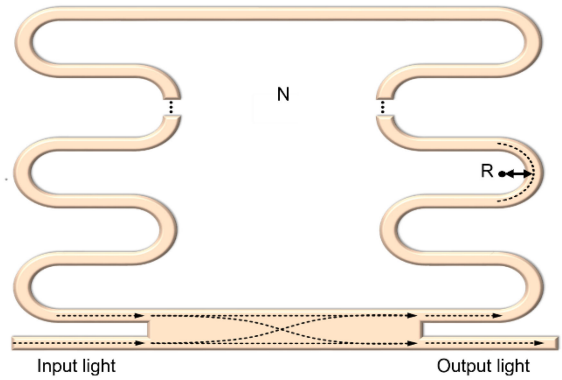

Fig. 1. Schematic of the S-bend resonator where N is the number of bending waveguide layers and R is the radius of the bending waveguide.

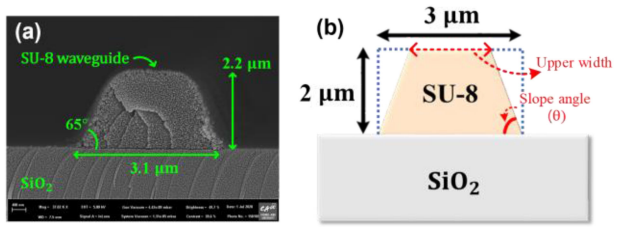

Fig. 2. (a) Cross-sectional field-emission scanning electron microscopy image of the fabricated MMW with thermal reflow, and (b) model of MMW with slope angle (θ).

assumes a round shape due to surface tension as it melts from the edge of the photoresist because of continuous heat or high temperature. Thus, the waveguide constituting the resonator is fabricated differently from the designed structure [17]–[19]. In addition, this phenomenon is exacerbated by overdevelopment. This mismatch with the originally designed structure changes the resonance characteristics of the resonator. Furthermore, with an increase in the severity of thermal reflow, the waveguide sidewall angle decreases, which results in a greater change in the resonance characteristics of the resonator. If a slope is formed on the sidewall of the waveguide, the confinement factor (CF) of the propagation mode decreases, and the light loss increases. This increase in light loss can deteriorate the extinction ratio (ER) and Q-factor of the resonator. Conversely, an increase in light loss indicates an increase in the range and intensity of evanescent waves, and this can enhance the sensitivity of the resonator. Therefore, a trade-off between the light loss and the sensitivity of the resonator is expected, and a detailed analysis with respect to the optimized angle of the sidewall slope is required.

In this study, analysis was performed using MODE solution based on the variational finite-difference time-domain by Lumerical Inc. First, the sidewall slope angle (θ) was defined by modeling the cross-section of the waveguide by thermal reflow. Then, the characteristic change of the MMW, the multi-mode interference (MMI), and the bending waveguide constituting the S-bend resonator were analyzed with respect to the θ. Finally, we investigated the characteristics of the transmission spectrum of the S-bend resonator with respect to changes in the θ of the waveguide.

II. Analysis of Sidewall Slope Effect in MMW on the S-Bend Resonator

As shown in Fig. 1, the S-bend resonator consists of a MMI coupler and bending structure based on the MMW [14]. Different from the SMW-based resonator, higher-order modes may be present in the waveguide of the S-bend resonator. The S-bend resonator uses mode discrimination in a multi-bending structure to eliminate higher-order modes of light. Mode discrimination is a phenomenon in which higher-order modes are removed based on the differences in the effective refractive index and losses between the fundamental mode and higher-order modes [14]. In this study, we considered an MMW-based S-bend resonator based on an SU-8 polymer, which can be fabricated through a photolithography process at a low cost. The low-viscosity SU-8 2002 polymer was used because the waveguide width and height could be designed with a low aspect ratio of several micrometers. Changes in the waveguide sidewalls or fabrication mismatches can influence the performance and characteristics of the resonator. Therefore, it is necessary to analyze the internal higher-order mode change and the performance of the S-bend resonator depending on the cross-sectional shape of the waveguide.

A. Analysis of Mode Profiles in an MMW

Because of thermal reflow and overdevelopment, the width of the waveguide gradually decreased from the bottom to the top formed the sidewall slope. A cross-section of the waveguide was approximated with a trapezoidal structure for simple analysis, and each structure of the S-bend resonator was analyzed based on θ. Fig. 2(a) presents a field-emission scanning electron microscopy image of a cross-section of the waveguide with a slope in the sidewalls caused by thermal reflow, and (b) illustrates the ideal waveguide structure (blue dotted line) and an approximated trapezoidal waveguide structure.

If the sidewall of the waveguide is fabricated with a sloped structure, the characteristics of the waveguide, such as the number of modes and confinement factor (CF), are different from the ideal condition ($\theta = 90°$). The nominal waveguide was assumed to have a width and height of 3 μm and 2 μm, respectively, and the refractive indices of the SU-8 and SiO_2 substrates were assumed to be 1.57 and 1.46, respectively (at 1550 nm) [20]. The CF of cross-sectional MMW was obtained using the definition of the following equation.

$$CF = \frac{Power\ of\ waveguide}{Total\ guided\ power} = \frac{\iint_{inside}^{Re}\left(\vec{E}\times\vec{H}^{*}\right)\cdot\hat{z}dxdy}{\iint_{total}^{Re}\left(\vec{E}\times\vec{H}^{*}\right)\cdot\hat{z}dxdy} \quad (1)$$

Fig. 3 presents the number of modes, the electric field (E-field) profile of each mode, and the CF with respect to θ. The waveguides were analyzed at intervals of 5° from 90° to a minimum of 60°, given that the loss of higher-order modes was large or non-existent when $\theta < 60°$. There were eight modes

(CF : Confinement factor) (RI : Refractive index)

Slope angle \ Mode	TE0	TM0	TE1	TM1	TE2	TM2	TE3	TE4
90°								
CF	0.960	0.928	0.943	0.897	0.841	0.807	0.895	0.792
Effective RI	1.516	1.516	1.457	1.465	1.432	1.380	1.356	1.372
85°								
CF	0.958	0.924	0.929	0.879	0.838	0.723	0.857	0.758
Effective RI	1.513	1.515	1.448	1.460	1.424	1.369	1.335	1.356
80°								
CF	0.956	0.920	0.847	0.851	0.835	0.792	0.744	
Effective RI	1.511	1.512	1.440	1.452	1.425	1.320	1.352	
75°								
CF	0.952	0.913	0.877	0.809	0.831	0.704		
Effective RI	1.507	1.510	1.427	1.444	1.421	1.305		
70°								
CF	0.946	0.902	0.823	0.748	0.866			
Effective RI	1.503	1.506	1.415	1.434	1.415			
65°								
CF	0.936	0.885	0.831	0.663	0.809			
Effective RI	1.497	1.501	1.402	1.424	1.405			
60°								
CF	0.919	0.856	0.787	0.560	0.779			
Effective RI	1.489	1.495	1.389	1.415	1.388			

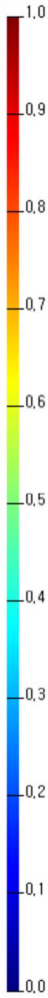

Fig. 3. E-field intensity profiles ($|E|^2$), CF and effective RI of the propagation modes of MMW with respect to θ.

in the designed rectangular waveguide. With a decrease in θ, the upper width decreased, thus resulting in a relatively small waveguide width. As expected, the number of modes present inside the smaller waveguide width decreased. From $\theta = 80°$ downward, several higher-order modes were eliminated, and only five modes were present in the waveguide with $\theta = 60°$. Furthermore, with a decrease in θ, the CF, which is the power ratio of the modes in the core area, decreased in the same mode, as shown in Fig. 3. When $\theta = 90°$, the CFs were 96% and 92.8% in the TE0 and TM0 modes, respectively. Moreover, when $\theta = 60°$, the CFs in the same mode were 91.9% and 85.6%, respectively. The CF differences were 3.9% in the TE0 mode and 7.2% in the TM0 mode. In the TE1 and TM1 modes, when $\theta = 90°$, the CFs were 94.3% and 89.7%. When $\theta = 60°$, the CFs were 78.7% and 56.0%, respectively, and the CF differences were 15.6% and 33.7%, respectively. These results indicate that the decrease in the CF due to structural changes was greater in higher-order modes than in the fundamental mode, thus resulting in more loss of light in higher-order modes within the same structure. Therefore, the relatively large loss of higher-order modes according to the reduction of θ may influence the mode discrimination phenomenon.

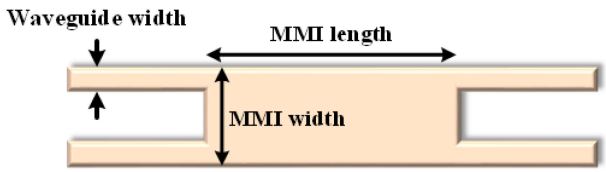

Fig. 4. Schematic of the multi-mode interference.

B. Characteristic Analysis of MMI and Bending Waveguide With Respect to the Sidewall Slope Angle

Fig. 4 presents the schematic of the MMI coupler constituting the S-bend resonator. The width and height of the MMI were 10 μm and 203 μm, respectively. It was designed for a 50:50 coupling ratio of waveguides with vertical sidewalls. When the S-bend resonator was fabricated through the photolithography

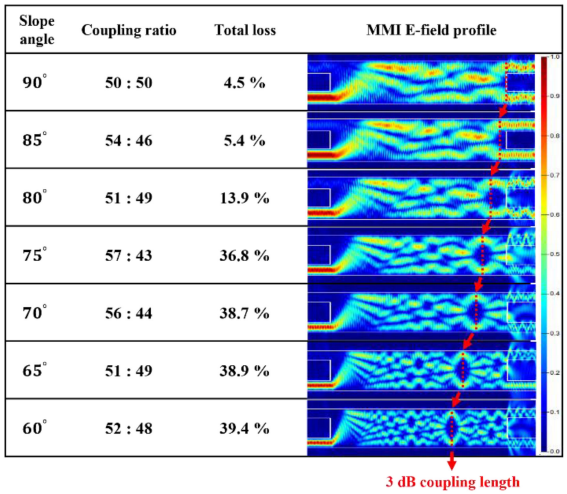

Fig. 5. Coupling ratio, total loss, and E-field intensity profiles ($|E|^2$) of MMI with respect to θ with an MMI length of 203 μm.

of the SU-8 polymer, the MMI characteristics were analyzed by θ generated in the waveguide. Fig. 5 presents the coupling ratio, total loss, and E-field profile of the MMI with respect to θ. A reduction in θ decreased the coupling length of 3 dB, which satisfied the 50:50 coupling ratio, thus resulting in back-reflection and an increase in the total loss of the MMI output power. In particular, the total loss increased significantly at angles of $\theta = 75°$ or less. However, given that the coupling ratio of the MMI did not deviate significantly from 50:50, the MMI can be used as a coupler.

The deformation in the shape of the waveguide can influence the light loss of each propagation mode within the bending waveguide. Thus, the bending loss of each mode was analyzed with respect to θ and the number of bending waveguides. Fig. 6(a) presents a schematic of the bending waveguide with a radius of 10 μm. Fig. 6(b) and (c) indicate the loss with respect to the slope angle θ of the bending waveguide in the TE0 and TM0 modes, which are fundamental modes, and the TE1 and TM1 modes, which are higher-order modes.

When the light passed through the bending waveguide once, the losses of the TE0 mode were 1.9% and 5.6% at $\theta = 90°$ and $\theta = 60°$, respectively, and the difference in the losses was only 3.7%. On the other hand, the losses of the TE1 mode were 8.6% and 35.2% at $\theta = 90°$ and $\theta = 60°$, respectively. When $\theta > 70°$, the loss of the TE1 mode rapidly increased, and the loss difference between $\theta = 90°$ and $\theta = 60°$ was 26.6%, which was much larger than that of the TE0 mode.

When passing through the bending waveguide six times, the losses of the TE0 mode were 24.9% and 58.4% at $\theta = 90°$ and $\theta = 60°$, respectively, and the difference in the losses was 33.5%. The losses of the TE1 mode were 39.7% and 93.7% at $\theta = 90°$ and $\theta = 60°$, respectively, and the difference in the losses was 54.0%. As shown in Fig. 6(c), a similar tendency is also observed for the TM mode. The above results demonstrate that the bending loss increases as θ is reduced. Above all, regardless of θ, there is still a difference in bending loss in the fundamental mode and second-order mode, which means that mode discrimination could occur. At $\theta = 80°$, a large bending loss occurs due to a phenomenon such as a mode conversion, but in Fig. 6(b) and (c), it can be seen that the tendency of bending loss inversely proportional to θ is maintained.

III. Analysis of Transmission Spectrum and Discussion

Fig. 7 presents the transmission spectra of the S-bend resonator at a center wavelength of 1550 nm with respect to θ and the number of bending waveguides. The intensity of the transmission spectrum is defined as a normalized value ranging from 0 to 1. The black and red lines represent the transmission spectrum of the resonator at external refractive indices of 1.00 and 1.01, respectively. The sensitivity of the resonator was obtained from the shift in the resonance wavelength. To precisely compare the output performance of the resonator with respect to θ, the comprehensive results of the Q-factor, free spectral range (FSR), ER, and sensitivity of the transmission spectrum were obtained, as shown in Fig. 8. The CF decreased as the θ of the waveguide decreased, as can be seen from Fig. 3. The decrease in the CF caused an increase in the propagation loss of light, which led to a decrease in the ER. When N = 3 (six bending structures), the ER was 8.88 dB at $\theta = 90°$ and 2.60 dB at $\theta = 60°$. Meanwhile, the Q-factor decreased with an increase in the propagation loss of light. In Fig. 8(a), when N = 3, the Q-factor at an ideal θ (90°) was 2.1×10^3, whereas at $\theta = 60°$, it decreased to 0.6×10^3. The trends of the Q-factor and ER with respect to θ are shown in Fig. 8(a) and (c), respectively. In contrast, with a decrease in θ, the sensitivity of the resonator gradually increased. When N = 3, the sensitivity was 25 nm/RIU at an ideal θ and 98 nm/RIU at $\theta = 60$ °. Given that the intensity of the evanescent field near the waveguide increased as the CF decreased, the resonator was more sensitive to changes in the refractive index outside the waveguide.

The sensitivity of the resonator increased as θ decreased, as shown in Fig. 8(b). Given that the FSR of a resonator is related only to the wavelength of light and length of the resonator, it is not influenced by the sidewall slope of the waveguide and is therefore constant. The Q-factor, ER, FSR, and sensitivity exhibited the same trend for N = 3 as that for other values of N. In Fig. 2(a), the θ of the waveguide constituting the resonator was 65°, and the ER of the corresponding transmission spectrum was smaller than that of the resonator at $\theta = 90°$. However, the sensitivity was higher than that at $\theta = 90°$. Thus, even when θ is approximately 65°, it can be used as a resonator sensor.

Based on the results presented above, there is a trade-off relationship between the Q-factor, ER, and sensitivity of the resonator. If the ER and Q-factor of the resonator transmission spectrum decrease due to a decrease in θ, it can be difficult to distinguish the resonance wavelength shift. However, the sensitivity of the resonator can be increased, and the material can be detected more effectively. Therefore, we have considered that it is able to present a tolerance range for θ referencing this trade-off relationship when we fabricate a multi-mode waveguide-based resonator.

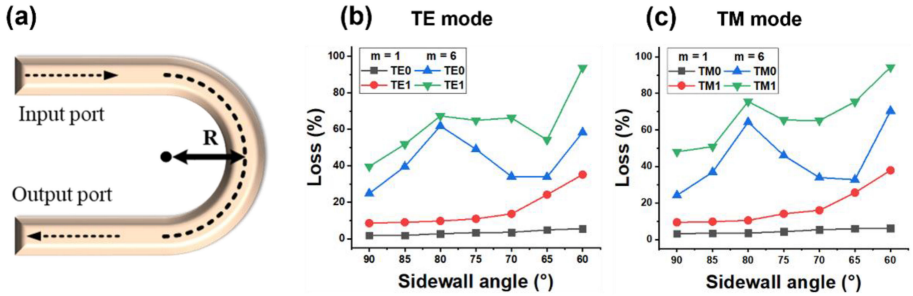

Fig. 6. (a) Bend structure of the waveguide with radius R; losses of fundamental and second-order (b) TE and (c) TM modes when light passes bend waveguide (m: the number of bending waveguide).

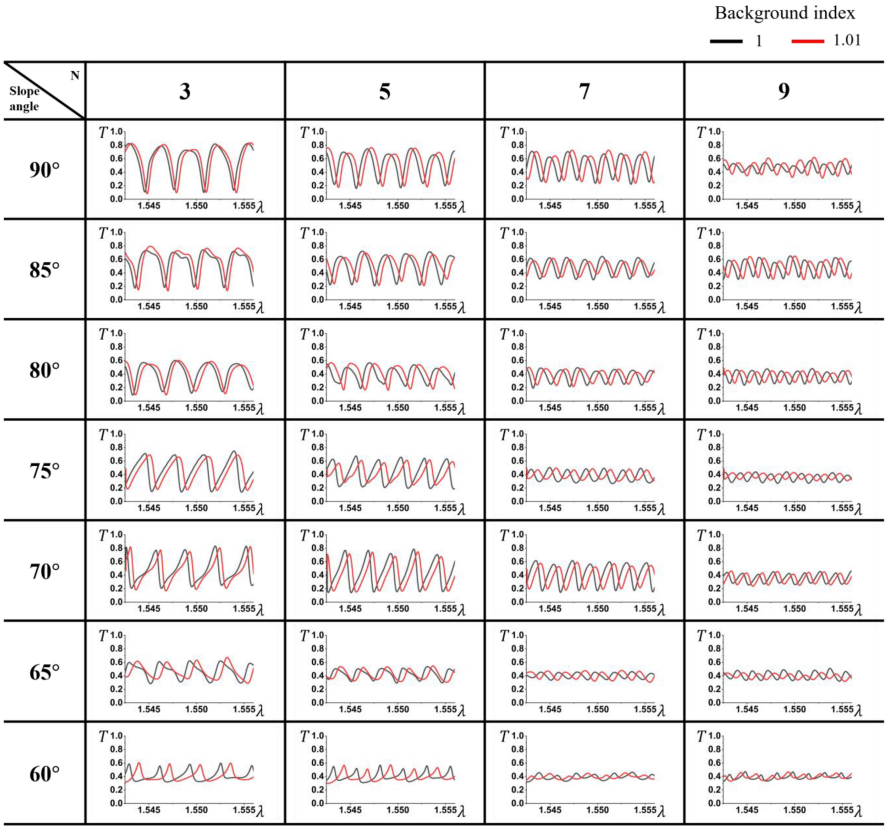

Fig. 7. Transmission spectra of the S-bend resonators with respect to the θ and the number of bending waveguides. The x-axis and y-axis represent wavelength (λ) from 1.525 μm to 1.56 μm and normalized transmission intensity (T), respectively. The black and red lines of the graph represent the transmission spectrum when the external refractive indices are 1 and 1.01, respectively.

IV. Conclusion

In this study, we analyzed the performance of an S-bend resonator with respect to the slope angle θ of the waveguide due to the thermal reflow of a low viscosity SU-8 polymer. It was found that the slope angle θ of the MMW decreased the number of propagation modes and the CF inside the waveguide. This decrease results in a decrease in the Q-factor and ER of the transmission spectrum in the S-bend resonator. Moreover, a decrease in the sidewall angle θ increases the extent and intensity of the evanescent field. This leads to an enhancement of the sensitivity of the resonator due to changes in the external refractive index. As a result, when the θ of the MMW was reduced from 90° to 65°, the ER and Q-factor decreased by 54% and 37% on average, respectively. However, the sensitivity of the resonator was increased by a factor of approximately 1.8 due to an increase of range and intensity in the evanescent field of the waveguide. Therefore, it was concluded that there may be a trade-off between the light loss due to the sidewall slope and the sensitivity of the resonator. If the appropriate value of the sidewall angle of MMW is determined by adjusting the hard bake time, we think the resonator sensor can be ideally used depending on the application field. The analysis results can serve

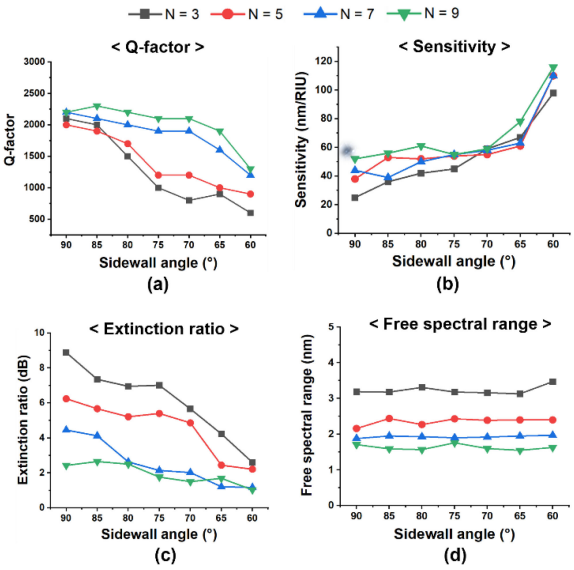

Fig. 8. Performance of the S-bend resonator with respect to θ: (a) Q-factor, (b) sensitivity, (c) ER, and (d) FSR.

as a criterion for determining the tolerance of θ in the MMW corresponding to a higher sensitivity of the sensor. The appropriate application of this tolerance can render the MMW-based optical sensor more insensitive to process errors, thus increasing the ease of fabrication of optical sensors. Moreover, the findings of this study can serve as a basis for further research on MMW-based optical sensors using polymer materials.

REFERENCES

[1] T. D. Martins *et al.*, "New insights on optical biosensors: Techniques, construction and application," *Intech*, 2013.

[2] M. Sumetsky, "Optimization of optical ring resonator devices for sensing applications," *Opt. Lett.*, vol. 32, no. 17, pp. 2577–2579, Sep. 2007, doi: 10.1364/OL.32.002577.

[3] X. Cheng, J. Hong, A. M. Spring, and S. Yokoyama, "Fabrication of a high-Q factor ring resonator using LSCVD deposited Si_3N_4 film," *Opt. Mater. Exp.*, vol. 7, no. 7, pp. 2182–2187, Jul. 2017, doi: 10.1364/OME.7.002182.

[4] L. Zhang and D. Dai, "Silicon subwavelength-grating microdisks for optical sensing," *IEEE Photon. Technol. Lett.*, vol. 31, no. 15, pp. 1209–1212, Aug. 2019, doi: 10.1109/LPT.2019.2922230.

[5] M. Kitsara, K. Misiakos, I. Raptis, and E. Makarona, "Integrated optical frequency-resolved Mach-Zehnder interferometers for label-free affinity sensing," *Opt. Exp.*, vol. 18, no. 8, pp. 8193–8206, Apr. 2010, doi: 10.1364/OE.18.008193.

[6] W. Gao *et al.*, "Refractive index and temperature sensor based on optical fiber Mach–Zehnder interferometer with trapezoid cone," *Opt. Eng.*, vol. 58, no. 5, May. 2019, Art. no. 057102, doi: 10.1117/1.OE.58.5.057102.

[7] H. Y. Choi *et al.*, "Miniature fiber-optic high temperature sensor based on a hybrid structured Fabry–Perot interferometer," *Opt. Lett.*, vol. 33, no. 21, pp. 2455–2457, Nov. 2008, doi: 10.1364/OL.33.002455.

[8] K. R. Kribich *et al.*, "Novel chemical sensor/biosensor platform based on optical multimode interference (MMI) couplers," *Sens. Actuators B Chem.*, vol. 107, no. 1, pp. 188–192, May. 2005, doi: 10.1016/j.sub.2004.11.098.

[9] P. Singh, "SPR biosensors: Historical perspectives and current challenges," *Sens. Actuators B Chem.*, vol. 229, pp. 110–130, Jun. 2016, doi: 10.1016/j.sub.2016.01.118.

[10] A. N. Nordin, "Optical-resonator-based biosensing systems: Current status and future prospects," *Nanobiosens. Dis. Diagn.*, vol. 5, pp. 41–50, Jun. 2016, doi: 10.2147/NDD.S70385.

[11] A. C. Ruege and R. M. Reano, "Multimode waveguides coupled to single mode ring resonators," *J. Lightw. Technol.*, vol. 27, no. 12, pp. 2035–2043, Jun. 2009, doi: 10.1109/JLT.2008.200651.

[12] F. Zhang and J. W. Y. Lit, "Direct-coupling single-mode fiber ring resonator," *J. Opt. Soc. Amer. A*, vol. 5, no. 8, pp. 1347–1355, Aug. 1988, doi: 10.1364/JOSAA.5.001347.

[13] A. Madani, H. Azarinia, and H. Latifi, "Design and fabrication of a polymer micro ring resonator with novel optical material at add/drop geometry using laser beam direct write lithography technique," *Optik*, vol. 124, no. 14, pp. 1746–1748, Jul. 2013, doi: 10.1016/j.ijleo.2012.06.003.

[14] D.-H. Kim, S.-J. Jeon, J.-S. Lee, S.-H. Hong, and Y.-W. Choi, "Novel S-Bend resonator based on a multi-mode waveguide with mode discrimination for a refractive index sensor," *Sensors*, vol. 19, no. 16, 2019, Art. no. 3600, doi: 10.3390/s19163600.

[15] M. Eryürek *et al.*, "Integrated humidity sensor based on SU-8 polymer microdisk microresonator," *Sens. Actuators B Chem.*, vol. 242, pp. 1115–1120, Apr. 2017, doi: 10.1016/j.snb.2016.09.136.

[16] D. Dai, L. Yang, Z. Sheng, B. Yang, and S. He, "Compact microring resonator with $2\times\times2$ tapered multimode interference couplers," *J. Lightw. Technol.*, vol. 27, no. 21, pp. 4878–4883, Nov. 2009, doi: 10.1109/JLT.2009.2030144.

[17] M.-K. Wei, I.-L. Su, M.-C. Jung, and K.-W. Huang, "Real-time observation for the formation of microlens arrays fabricated using thermal reflow process," *J. Appl. Sci. Eng.*, vol. 7, no. 2, pp. 81–86, Jun. 2004, doi: 10.6180/jase.2004.7.2.05.

[18] M. Wang *et al.*, "A novel thermal reflow method for the fabrication of microlenses with an ultrahigh focal number," *RSC Adv.*, vol. 5, pp. 35311–35316, Apr. 2015, doi: 10.1039/c5ra00957j.

[19] Y. Zhao *et al.*, "Exploration of lift-off Ge–As–Se chalcogenide waveguides with thermal reflow process," *Opt. Mater.*, vol. 92, pp. 206–211, Jun. 2019, doi: 10.1016/j.optmat.2019.04.033.

[20] K. Tung, W. Wong, and E. Pun, "Polymeric optical waveguides using direct ultraviolet photolithography process," *Appl. Phys. A*, vol. 80, pp. 621–626, Sep. 2003, doi: 10.1007/s00339-003-2248-8.